A Novel Power-Angle Control Method of DFIG-DC System Based on Regulating Air Gap Flux Vector

Wu, Chao; Zhou, Dao; Cheng, Peng; Blaabjerg, Frede

Published in:
I E E E Transactions on Power Electronics

DOI (link to publication from Publisher):
10.1109/TPEL.2020.3001967

Publication date:
2021

Document Version
Accepted author manuscript, peer reviewed version

A Novel Power-Angle Control Method of DFIG-DC System Based on Regulating Air Gap Flux Vector

Chao Wu, *Member, IEEE,* Dao Zhou, *Senior Member, IEEE,* Peng Cheng, and Frede Blaabjerg, *Fellow, IEEE*

***Abstract*—This paper presents a novel power-angle control method of DFIG-DC system based on regulating air gap flux vector. The relationship between the angle of air gap electromotive force (EMF) vector and stator output power is revealed in this paper, which can be used for controlling the output power directly. Since the stator frequency is determined by the rotating speed of air gap flux vector and the output power is determined by the angle of air gap EMF vector, the stator frequency can be generated by the power control loop which can avoid the classical voltage model or current model and reduce the parameter dependency. The stator frequency can be regulated through *d*-axis rotor current since the product of stator frequency and *d*-axis rotor current is constant. Furthermore, the improved direct resonant control for torque ripple and harmonic current mitigation can still be applied in this novel control method because air gap flux orientation is achieved through controlling the *q*-axis air gap flux to be zero. Finally, the experimental results are presented to validate the proposed control method.**

***Index Terms*— Doubly-fed induction generator, Air gap flux vector, Power angle control, Direct resonant control**

I. Introduction

Recently, there are growing research interests in the direct current (DC) transmission and connection of doubly fed induction generator (DFIG) based wind farm [1]-[4]. In the multiple existing topologies of DFIG connected to DC grid, the DFIG connected to DC grid through diode bridge on stator side has gained extensive attention and research due to its simple structure and smaller converter cost, which is also called as DFIG-DC system. However, the traditional vector control strategy based on the phase-locked loop (PLL) cannot be applied because there is no AC grid in the DFIG-DC topology and the stator frequency needs to be controlled additionally [5]. Thus, the primary objective of this topology is to achieve an accurate control of the stator frequency and output power. However, the basic problem encountered of this topology is how to obtain the stator frequency and orientation angle with as little parameter dependency as possible.

There are several research devoting in studying control strategies of this DFIG-DC system [6]-[15]. The decoupling control of stator frequency and stator power is mostly achieved through the stator flux orientation control. In these methods, the stator frequency and stator flux angle are indispensable for the decoupling control. According to the methods of obtaining the stator frequency and orientation angle, these existing methods can be generally divided into two categories: voltage model or current model.

In [6]-[8], the stator frequency and stator flux angle are obtained based on the stator voltage model. In [6]-[7], the stator frequency and stator flux angle are directly calculated based on the stator flux, which is highly dependent on the resistance parameters. Furthermore, the stator flux is the integral of stator voltage which is difficult to achieve in practical occasion due to an unavoidable dc sampling offset. In [8], the integral link is substituted by inertia link which can reduce the effect of dc sampling offset but can not eliminate the effect of dc sampling offset, which will cause a fundamental frequency ripple in the orientation angle.

In [9]-[12], the stator frequency and stator flux angle are acquired based on the current model. In [9], the magnitude of stator flux is applied for the stator frequency control, which is dependent on the stator inductance and mutual inductance. In [10]-[12], a stator flux PLL is proposed to obtain the stator frequency and stator flux angle by controlling the *q*-axis stator flux to be zero, which can avoid the calculation process but also dependent on the ratio of stator inductance and mutual inductance. When the DFIG-DC system is operating in the standalone mode, the dc voltage is also controlled based on stator flux orientation [13]-[15].

In conclusion, all these existing methods based on stator flux orientation control can not avoid the dc offset issue or parameter dependency. It can be found that there is no ac grid imposed on the stator side of DFIG and there is no reactive power flow to the dc grid, thus, the stator flux orientation control and decoupling control of stator frequency and stator power are not

Manuscript received October 9, 2019; revised February 18, 2020; accepted Jun 10, 2020. This work was supported THE VELUX FOUNDATIONS under the VILLUM Investigator Grant REPEPS (Award Ref. No.: 00016591) and in part by the National Natural Science Foundation of China under Grant 51807182 (*Corresponding author: Peng Cheng*).

Chao Wu, Dao Zhou and Frede Blaabjerg are with the Department of Energy Technology, Aalborg University, Aalborg 9220, Denmark (e-mail: cwu@et.aau.dk, zda@et.aau.dk and fbl@et.aau.dk).

Peng Cheng is with the China Institute of Energy and Transportation Integrated Development, North China Electric Power University, Beijing, 102206, China (e-mail: p.cheng@ncepu.edu.cn)

necessary for this topology.

Totally different from the existing DFIG-DC control methods, the stator frequency and stator power are not decoupling control through the *d-q* axis rotor current. The relationship between the stator power and angle of air gap EMF is established. The stator power is not controlled by the rotor current on the active axis, but controlled by the angle between air gap voltage and stator side voltage. In this way, the stator frequency and orientation angle are obtained based on the stator active power control loop, which can avoid the voltage model and current model. Furthermore, the air gap flux orientation method is achieved by controlling the *q*-axis exciting current to zero. Through regulating the air gap flux vector, the stator frequency and stator active power can both be controlled accurately without parameter dependency and avoid the sampling offset problem.

Since the stator voltage is highly distorted, the harmonic currents will cause torque ripple which should be reduced. In [16]-[17], predictive control methods are proposed for suppressing torque ripples. However, these literatures are just aimed at the torque ripple suppression without considering the harmonic currents in stator and rotor winding. An improved direct resonant control method is proposed for suppressing the torque ripples and mitigating harmonic currents simultaneously [18]. In this paper, since the rotating frame is aligned with the air gap flux vector, the improved direct resonant control method is still suitable in this novel control method, which can mitigate the torque ripple and harmonic currents simultaneously.

In conclusion, the novel frequency and power control method can avoid the parameter dependency. Moreover, all the existing direct resonant control for improving the performance can still be applied directly.

The rest of paper is organized as follows. The system configuration and mathematical model are described in section II. The detailed control strategy of rotor side converter (RSC) is elaborated in detail in section III. Furthermore, the performance analysis of power-angle control and improved direct resonant control are presented in section IV. Section V shows the experimental results and the conclusion is made in section VI.

II. System Configuration and Mathematical Model

A. System Configuration

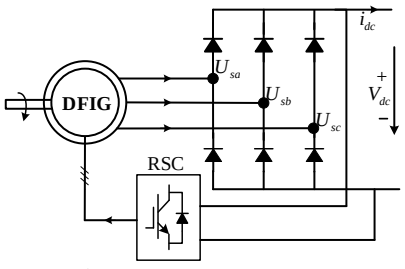

Fig. 1. Configuration of DFIG-DC system. Diode bridge on the stator side, PWM converter on the rotor side.

The DFIG-DC system topology is graphically shown as Fig. 1, where U_{sabc} represents the stator voltage, V_{dc} represents the dc link voltage and i_{dc} represents the dc side current. The working principle of DFIG to generate power to DC grid can be elaborated as: firstly, the rotor side exciting current is injected to rotor winding through RSC, then the air gap EMF is built. When the peak value of the phase-phase air gap EMF is higher than the dc voltage, the diode bridge is conducting and the DFIG injects power to dc grid.

B. Mathematical model

As shown in Fig. 1, the reference direction of stator current and rotor current are defined in terms of the generator mode. According to the equivalent circuit of the DFIG under the synchronized *d-q* reference frame, the air gap flux vector can be expressed as:

$$\boldsymbol{\psi}_{mdq} = L_m\left(-\boldsymbol{I}_{sdq} + \boldsymbol{I}_{rdq}\right) \tag{1}$$

where $\boldsymbol{\psi}_{mdq}$ is air gap flux vector, $\boldsymbol{I}_{sdq}$, $\boldsymbol{I}_{rdq}$ are the stator and rotor current vector, L_m is mutual magnetic inductance.

In the steady state, the air gap EMF can be given as,

$$\boldsymbol{E}_{mdq} = j\omega_s\boldsymbol{\psi}_{mdq} \tag{2}$$

where ω_s is the stator frequency.

Seen from the air gap side, the steady state equivalent circuit of the DFIG-DC system can be seen as Fig. 2, where R_s is stator resistance and $L_{\sigma s}$ is the stator leakage inductance.

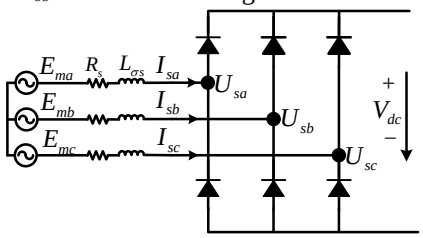

Fig. 2. Steady state equivalent circuit of the DFIG-DC system.

When the diode bridge is working at the continuous conduction mode, the stator voltage is a three-step square wave and the magnitude of stator fundamental voltage can be calculated as [8],

$$U_{s1} = \frac{2}{\pi}V_{dc} \tag{3}$$

According to (3), the stator fundamental voltage is a fixed value since the dc link voltage is constant. Thus, the stator voltage can be considered as a constant voltage source when ignoring the harmonics. The stator resistance is much smaller compared with the electrical impedance of leakage inductance and it can be ignored. The power transferred from the DFIG to dc grid can be described as Fig. 3(a) and the phasor diagram can be seen as Fig. 3(b). The phasor diagram is in the synchronous *d-q* frame. The phase angle between the stator fundamental voltage vector and the air gap EMF vector is δ. Moreover, the stator fundamental current vector is the same phase with stator voltage vector due to the diode bridge [5]. The amplitude of the air gap EMF vector is E_m. Thus, the stator active power transferred from DFIG to the DC grid can be calculated as,

$$P_s = \frac{E_m U_{s1}}{\omega_s L_{\sigma s}}\sin\delta = \frac{\psi_m U_{s1}}{L_{\sigma s}}\sin\delta \tag{4}$$

Since the stator leakage inductance is small, the amplitude of air gap EMF is almost the same as the stator fundamental voltage. The stator active power can be controlled by the phase

This article has been accepted for publication in a future issue of this journal, but has not been fully edited. Content may change prior to final publication. Citation information: DOI 10.1109/TPEL.2020.3001967, IEEE Transactions on Power Electronics

angle between air gap EMF and stator voltage vector, which can be used for obtaining the stator frequency and orientation angle in the system.

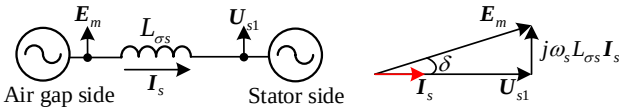

Fig. 3. Equivalent phasor diagram of DFIG-DC system.
(a) equivalent diagram of power transfer (b) phasor diagram

The stator active power is calculated by the dot product of stator voltage vector and stator current vector,

$$P_s = \mathrm{Re}\left(\boldsymbol{U}_{sdq} \cdot \boldsymbol{I}_{sdq}\right) = U_{sd} I_{sd} + U_{sq} I_{sq} \tag{5}$$

The torque can be calculated by the cross product of air gap flux and rotor current as,

$$T_e = \mathrm{Re}\left(j\boldsymbol{\psi}_{mdq} \hat{\boldsymbol{I}}_{rdq} \right) = L_m \left(I_{sq} I_{rd} - I_{sd} I_{rq} \right) \tag{6}$$

The harmonic components existed in both the stator and rotor current result in the torque ripple. The detailed expression of torque ripple has been deduced in [15], which is not discussed in this paper.

III. Control Strategy

Since the dc voltage is constant, the control objective of the RSC is to achieve accurate regulation of output power to dc grid. Furthermore, the stator frequency of the DFIG is not imposed by ac grid, which also needs to be controlled additionally.

The RSC control scheme for the stator power and stator frequency regulation is shown as Fig. 4, which mainly consists of the stator power control, stator frequency control, air gap flux orientation and current control. The current control is the inner control loop, which is the same with conventional current control and not repeated here. The stator power control, stator frequency control and air gap flux orientation, improved direct resonant control will be elaborated in detail in the following three parts.

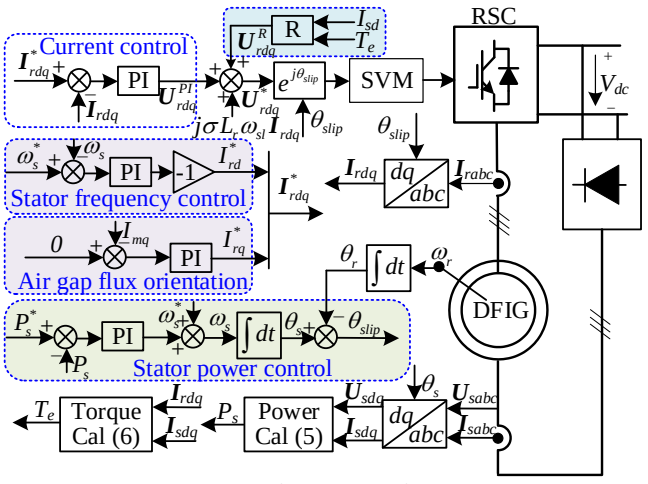

Fig. 4. RSC control scheme for power and frequency regulation.

A. Stator power control

As can be seen from (4), the stator power will increase with higher angle δ, which is the integral of rotating speed deviation between air gap EMF and stator voltage vector. Besides, as the angle δ will increase with the higher stator frequency, the stator frequency can be generated by power control loop as,

$$\omega_s = \frac{k_{pp} s + k_{ip}}{s} \left(P_s^* - P_s \right) \tag{7}$$

where k_{pp} and k_{ip} are the proportional gain and integral gain of the power loop controller.

The orientation angle is the integral of stator frequency which can be expressed as,

$$\theta_s = \frac{1}{s} \omega_s \tag{8}$$

B. Stator frequency control and air gap flux orientation

According to the air gap flux expressed in (1), the q-axis exciting current corresponding to q-axis air gap flux can be expressed as

$$I_{mq} = I_{rq} - I_{sq} \tag{9}$$

In order to achieve the air gap flux orientation, the q-axis air gap flux should be controlled to zero. Thus, the reference of q-axis rotor current can be expressed as,

$$I_{rq}^* = \frac{k_{pf} s + k_{if}}{s} \left(0 - I_{mq} \right) \tag{10}$$

where k_{pf} and k_{if} are the proportional gain and integral gain of the q-axis exciting current controller.

Since the air gap flux vector is orientated in d-axis, the magnitude of stator flux can be approximatively calculated as,

$$\left|\boldsymbol{\psi}_s\right| \approx \left|\boldsymbol{\psi}_m\right| = L_m \left(I_{rd} + \left|\boldsymbol{I}_s\right| \sin\delta \right) \approx L_m I_{rd} \tag{11}$$

Since the product of stator frequency and stator flux is the magnitude of stator fundamental voltage, according to (3) and (11), the relationship between d-axis rotor current and stator frequency can be expressed as,

$$\omega_s \approx \frac{2V_{dc}}{\pi L_m I_{rd}} \tag{12}$$

As can be seen from (12), the stator frequency is inverse ratio with d-axis rotor current. Thus, the reference of d-axis rotor current can be given as,

$$I_{rd}^* = -\frac{k_{pf} s + k_{if}}{s} \left(\omega_s^* - \omega_s \right) \tag{13}$$

where k_{pf} and k_{if} are the proportional gain and integral gain of the stator frequency controller, which are the same as the q-axis exciting current controller since these two loops are both outer loop for generating rotor current reference.

C. Improved direct resonant control

The detailed mathematical model of DFIG-DC system is built in [15], and the dominant harmonics in air gap flux and stator current are fifth and seventh harmonic. Thus, the main torque ripple becomes sixth order harmonic and a resonant controller can be applied to mitigate the torque ripple. The repetitive controller can also be applied to suppress all the torque ripples if all harmonics are considered. In this paper, only a resonant controller is applied since it is just to prove that the direct resonant control strategy can also be used in this novel power

angle control strategy.

The transfer function of the resonant controller used in this paper can be expressed as,

$$G_R(s)=\frac{2k_r\omega_c s}{s^2+2\omega_c s+(6\omega_s)^2} \tag{14}$$

where ω_c is the cutoff frequency and k_r is the gain of the resonant controller. The cutoff frequency is applied to take the stator frequency fluctuation into account, the range of which is always designed from 5 to 15 rad/s. It is noted that 10 rad/s is used in this paper.

The rotor harmonic voltage for mitigating torque ripple and harmonic currents can be expressed as,

$$\boldsymbol{U}_{rdq}^{R}=G_R(s)\left(I_{sd}^{*}-I_{sd}\right)+jG_R(s)\left(T_e^{*}-T_e\right) \tag{15}$$

In (15), both the I_{sd}^{*} and T_e^{*} are set as zero to mitigate the *d*-axis stator harmonic current and torque ripple.

Finally, the total rotor voltage reference can be expressed as,

$$\boldsymbol{U}_{rdq}^{*}=\boldsymbol{U}_{rdq}^{PI}+\boldsymbol{U}_{rdq}^{R}+j\sigma L_r\omega_{sl}\boldsymbol{I}_{rdq} \tag{16}$$

where $\boldsymbol{U}_{rdq}^{PI}$ is the output of the PI controller, $\boldsymbol{U}_{rdq}^{R}$ is the output of the direct resonant controller. ω_{sl} is the slip angular speed, σ is the leakage coefficient, $j\sigma L_r\omega_{sl}\boldsymbol{I}_{rdq}$ is the cross coupling term which is used as feedforward item.

IV. Control Performance Analysis

The RSC control scheme in Fig. 4 indicates that the stator frequency and stator power are non-decoupling control. The stator frequency is obtained by the power control loop. Thus, in order to analyze the control performance and stability of the power control loop and stator frequency control loop, these two loops should be considered together.

A. Stability of stator frequency and power control

According to (4), the stator active power can be expressed by stator voltage and *d*-axis rotor current as,

$$P_s=\frac{\psi_m U_{s1}}{L_{\sigma s}}\sin\delta\approx\frac{L_m U_{s1}}{L_{\sigma s}}I_{rd}\sin\delta \tag{17}$$

As can be seen from (17), the stator power is related to both the *d*-axis rotor current and angle δ. The effect of these two factors on the stator power can be expressed by the partial derivative as,

$$\frac{\partial P_s}{\partial I_{rd}}=\frac{L_m}{L_{\sigma s}}U_{s1}\sin\delta \tag{18}$$

$$\frac{\partial P_s}{\partial \delta}=\frac{L_m}{L_{\sigma s}}U_{s1}I_{rd}\cos\delta \tag{19}$$

Since the relationship between stator power and angle δ is non-linear, small signal model is deduced for the stability and control performance analysis. Assume the steady-state working point is P_{s0}, δ_0, I_{rd0}, the small signal model of power can be expressed as,

$$\Delta P_s=\left(\frac{L_m}{L_{\sigma s}}U_{s1}I_{rd}\cos\delta_0\right)\Delta\delta+\left(\frac{L_m}{L_{\sigma s}}U_{s1}\sin\delta_0\right)\Delta\left|I_{rd}\right| \tag{20}$$

The relationship between stator frequency and angle δ can be expressed as,

$$\Delta\delta=\frac{1}{s}\Delta\omega_s \tag{21}$$

Since the inner loop of the rotor current control is faster than the outer power control loop, it can be simplified as a unity gain block. Combining (20) and (21), the block diagram of the power control loop can be shown as Fig. 5.

According to Fig. 5, the characteristic equation of the power and stator frequency control system can be deduced as,

$$G_{open}=1+\frac{L_m U_{s1}}{L_{\sigma s}}\frac{k_{pp}s+k_{ip}}{s}\left(\frac{k_{pf}s+k_{if}}{s}\sin\delta_0+\frac{1}{s}I_{rd0}\cos\delta_0\right) \tag{22}$$

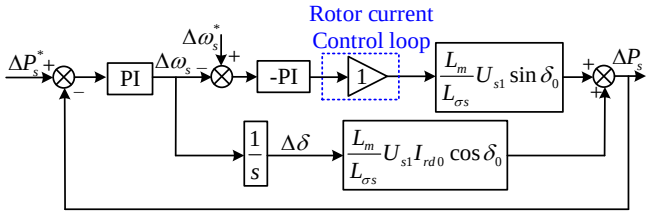

Fig. 5. Block diagram of power and stator frequency control loop.

Since the range of angle δ is quite small and near zero, sin δ is approximately zero during the whole power range. According to Fig. 5, the effect of stator frequency control on the power control can be eliminated. Thus, the operating point for designing the power control is the zero output power, which means that the angle δ is zero and sin δ is zero. In this way, the power control loop can be simplified as Fig.6.

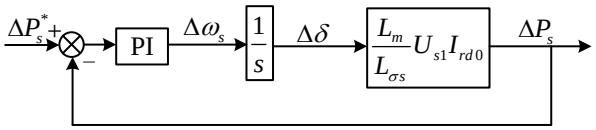

Fig. 6 Block diagram of the simplified power control loop.

The transfer function of stator power control loop can be deduced as,

$$\frac{\Delta P_s}{\Delta P_s^{*}}=\frac{ak_{pp}s+ak_{ip}}{s^2+ak_{pp}s+ak_{ip}}=\frac{2\xi\omega_n s+\omega_n^2}{s^2+2\xi\omega_n s+\omega_n^2} \tag{23}$$

where $a=L_m/L_{\sigma s}\cdot U_{s1}I_{rd0}$. As can be seen from the transfer function of power loop, it is a second order system. According to the design principle of second order system, the damping ratio ξ is always set as 0.707 and the bandwidth is designed based on the power control requirement. In this paper, the bandwidth of the stator power control is designed as 10 Hz. Thus, the ω_n is set as 20π rad/s. The proportional (k_{pp}) and integral (k_{ip}) parameters of power control loop can be obtained as 0.29 and 126, respectively. The proportional (k_{pf}) and integral (k_{if}) parameter of stator frequency control loop are set as 1 and 80, respectively.

According to the characteristic equation listed in (22), the root locus of stator power changing from zero to 1 pu is plotted in Fig. 7. The numbers smaller than 1 in the left side show the damping ratio ξ and the numbers in the right side represent the magnitude of the poles. It is obvious to see the poles move to the left side with the increase of stator power and all the poles are located in the left half plane, which indicates the power and stator frequency control loop are always stable. Furthermore,

This article has been accepted for publication in a future issue of this journal, but has not been fully edited. Content may change prior to final publication. Citation information: DOI 10.1109/TPEL.2020.3001967, IEEE Transactions on Power Electronics

the variation of poles with the stator power is not so significant, which indicates that the operating point has little effect on the power control performance. In order to further validate this viewpoint, the step response with different stator power operating points is shown in Fig. 8. The blue line is the step response of transfer function (23) and the red line is the simulation result of real model. The step response of different power change is consistent with the deduced transfer function from Fig. 6, which also corroborates with the root locus in Fig. 7.

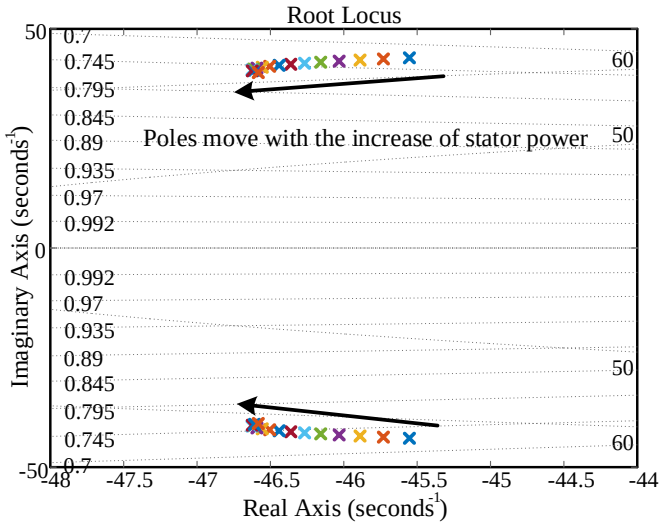

Fig. 7. Root locus of stator power and frequency control loop when stator power changes from 0 pu to 1 pu.

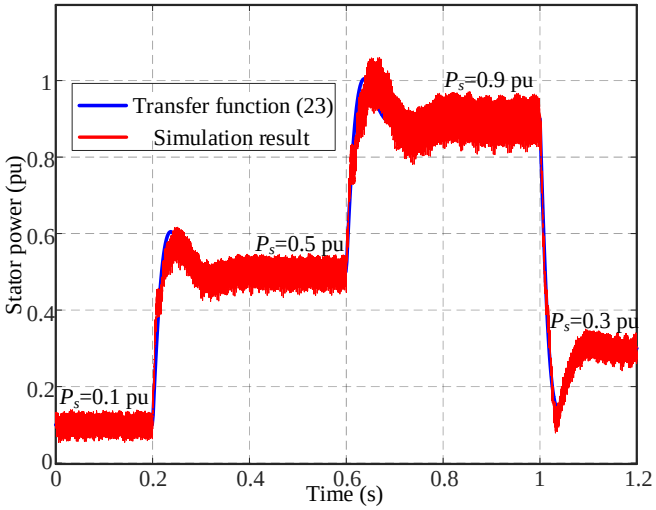

Fig. 8. Step response of different stator power change.

B. *Effectiveness of improved direct resonant control*

When the air gap flux vector is orientated at *d*-axis, the *q*-axis air gap flux Ψ_{mq0} is equal to zero. Thus, the torque expression in (6) can be expressed in detail as,

$$T_e = \left(\psi_{md0} I_{rq0}\right) + \left(\psi_{md0} I_{rq6} + I_{rq0}\psi_{md6} - I_{rd0}\psi_{mq6}\right) + \left(\psi_{md6} I_{rq6} - \psi_{mq6} I_{rd6}\right) \quad (24)$$

where Ψ_{md0} and Ψ_{mq0} express the air gap fundamental flux in *d*-*q* axis, Ψ_{md6} and Ψ_{mq6} express the sixth order air gap harmonic flux in *d*-*q* axis. I_{rd0} and I_{rq0} express the rotor fundamental flux in *d*-*q* axis, I_{rd6} and I_{rq6} express the sixth order rotor harmonic current in *d*-*q* axis.

The first term is average torque which is a constant dc value. The second term is harmonic components with different frequencies. The third term is product of smaller items which can be ignored. Thus, the dominant sixth order torque ripple can be expressed as,

$$T_{e6} = \psi_{md0} I_{rq6} + I_{rq0}\psi_{md6} - I_{rd0}\psi_{mq6} \quad (25)$$

As it can be seen from (24), the torque ripple is only affected by the *q*-axis rotor harmonic currents and has no relationship with *d*-axis rotor harmonic currents. Thus, the direct resonant control on *q*-axis can still be applied for mitigating torque ripple under the air gap flux orientation control.

The relationship of stator harmonic current and rotor harmonic current can be expressed as,

$$I_{sd6} = I_{rd6} - \frac{1}{L_m}\psi_{md6} \quad (26)$$

where I_{sd6} expresses the sixth order stator harmonic current in *d*-axis.

Since the stator harmonic current is linear with the rotor harmonic current, the resonant controller can be used to control the rotor harmonic current, indicating that the resonant controller can also be used to directly control the stator harmonic current. Thus, the *d*-axis stator harmonic current and torque ripple can be combined as a new complex variable. The direct resonant control of the new complex variable can be expressed as the transfer function shown in Fig. 9.

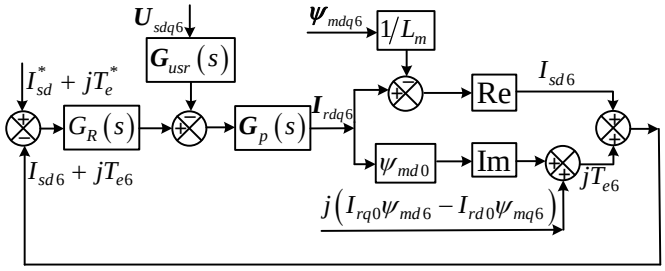

Fig. 9. Block diagram of improved direct resonant control.

The complex transfer function in Fig. 9 is obtained based on the DFIG model which can be expressed as,

$$\boldsymbol{G}_{usr}(s) = \frac{L_m}{L_s}\frac{s + j\omega_{sl}}{s + j\omega_s} \quad (27)$$

$$\boldsymbol{G}_p(s) = \frac{1}{R_r + \sigma L_r s} \quad (28)$$

where L_s is the stator inductance and R_r is rotor resistance. As can be seen from the plant transfer function $\boldsymbol{G}_p(s)$, there is no coupling term in the denominator, since the coupling term has been added to the rotor voltage as feedforward in (16).

As can be seen from Fig. 9, the *d*-axis stator harmonic current can be calculated as,

$$I_{sd6} = \mathrm{Re}\left(\frac{G_R(s)\boldsymbol{G}_p(s)}{1 + G_R(s)\boldsymbol{G}_p(s)}\left(I_{sd}^* + jT_e^*\right) + \frac{\boldsymbol{G}_{usr}(s)\boldsymbol{G}_p(s)}{1 + G_R(s)\boldsymbol{G}_p(s)}\boldsymbol{U}_{sdq6} - \frac{1}{L_m}\boldsymbol{\psi}_{mdq6} \right) \quad (29)$$

This article has been accepted for publication in a future issue of this journal, but has not been fully edited. Content may change prior to final publication. Citation information: DOI 10.1109/TPEL.2020.3001967, IEEE Transactions on Power Electronics

Since there is no imaginary part contained in the plant transfer function $\boldsymbol{G}_p(s)$, the *d*-axis stator harmonic current can be simplified as,

$$I_{sdh} = \frac{G_R(s)\boldsymbol{G}_p(s)}{1+G_R(s)\boldsymbol{G}_p(s)} I_{sdh}^* + \mathrm{Re}\left(\frac{\boldsymbol{G}_{usr}(s)\boldsymbol{G}_p(s)}{1+G_R(s)\boldsymbol{G}_p(s)} \boldsymbol{U}_{sdqh} - \frac{1}{L_m}\boldsymbol{\psi}_{mdqh} \right) \tag{30}$$

As can be seen from (30), the *d*-axis harmonic current has no relationship with the torque reference, which can validate the decoupling control of the *d*-axis harmonic current and torque ripple. On the other hand, only the *d*-axis harmonic current can be suppressed to zero since the *q*-axis harmonic current is used for mitigating torque ripple which can not be suppressed to zero. Thus, there is still some stator harmonic currents, the detailed analysis of stator and rotor harmonic currents of improved direct resonant control can be seen in [18].

V. Experimental Results

In order to validate the control strategy proposed in section III, a DFIG-based experimental system is developed. The schematic diagram of the experimental system is shown in Fig. 10. The DFIG was driven by a squirrel cage induction motor with general motor driver. The control strategy of the RSC is implemented on the TI TMS320F28335 DSP and the switching frequency is 10 kHz with a sampling frequency of 10 kHz. The parameters of the DFIG are shown in Table I. All the waveforms are acquired by a YOKOGAWA DL750 scope.

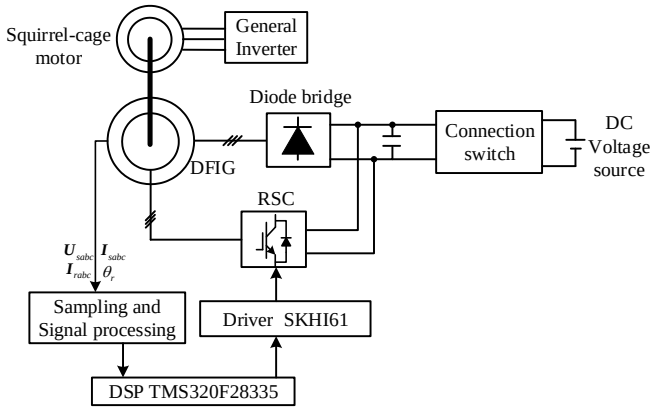

Fig. 10. Schematic diagram of the experiment system.

TABLE I Parameters of the tested DFIG

Parameters	*Value*	*Parameters*	*Value*
Rated power	1.0 kW	Rated voltage	110 V
Rated frequency	50 Hz	DC voltage	140 V
Pole pairs	3	R_s	1.01 Ω
R_r	0.88 Ω	L_m	87.5 mH
$L_{\sigma s}$	5.6 mH	$L_{\sigma r}$	5.6 mH

The experimental results of stator flux orientation control in [9] with dc sampling offset in rotor current is shown in Fig. 11. The stator power reference is 400 W. The stator frequency reference is 50 Hz and the rotor speed is 800 rpm. Thus, the dc offset in rotor current is expressed as 10 Hz pulsation component is the synchronous *d*-*q* frame, which will cause 10 Hz ripples in stator power and torque. As can be seen from the results, the envelope of stator current oscillates at 10 Hz. The 10 Hz ripples in stator power and torque are even higher than the 300 Hz ripples which need to be suppressed.

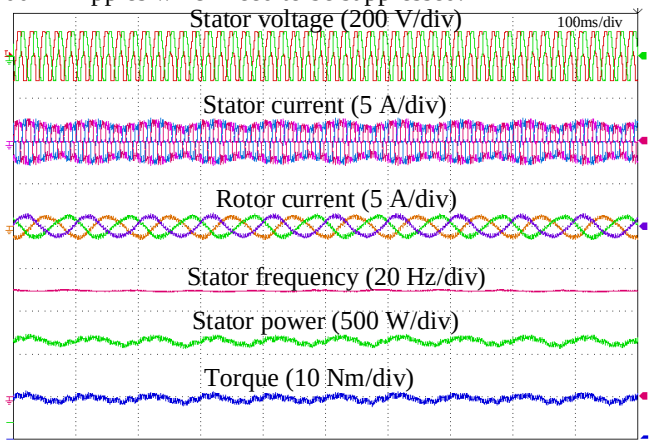

Fig. 11. Experimental results of stator flux orientation control with dc offset.

In the latter experimental results, the novel power and frequency control method is applied. As can be seen from Fig. 12, the 10 Hz ripples are eliminated.

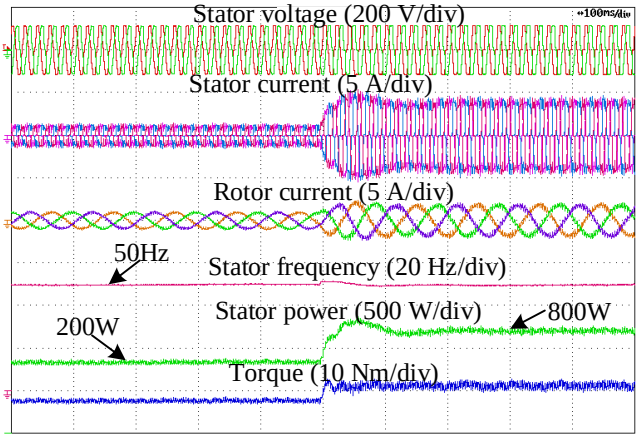

Fig. 12. Step response of power change from 200 W to 800 W.

Fig. 12 shows the step response of DFIG when the stator active power reference changes from 200 W to 800 W. The rotor speed is 800 rpm and the stator frequency is set as 50 Hz. The stator active power has a little overshoot since it is a second order system which is consistent with the theoretical analysis in section IV (A). On the other hand, it can track the power reference accurately in 110 ms without steady state error, which validates the effectiveness of stator power control loop.

The step response of the stator frequency change from 50 Hz to 60 Hz is shown in Fig. 13. The stator power reference is 500 W. During the change of stator frequency, the stator power has a pulsation which is caused by transient stator flux but will come to steady state in 50 ms. The stator frequency can quickly track the reference frequency in 10 ms without any overshoot which

This article has been accepted for publication in a future issue of this journal, but has not been fully edited. Content may change prior to final publication. Citation information: DOI 10.1109/TPEL.2020.3001967, IEEE Transactions on Power Electronics

validates the effectiveness of stator frequency control loop.

The zoomed view of left part in Fig.13 is shown in Fig. 14. The stator frequency is set as 50 Hz and stator power is set as 500 W. Due to the diode bridge on the stator side, the stator current is highly distorted with 5th and 7th order harmonics, which are 23.7% and 6.4%, respectively. The 300 Hz ripples in the torque is 6.8%, which is harmful for the mechanical shaft of DFIG. Thus, it is necessary to mitigate the harmonic currents and torque ripple using an improved direct resonant control.

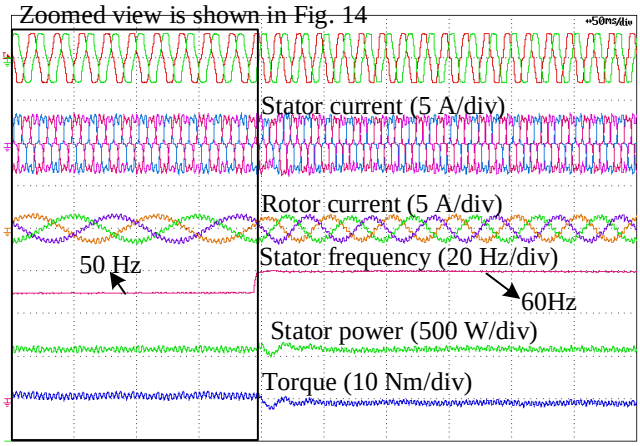

Fig. 13. Step response of stator frequency change from 50 Hz to 60 Hz.

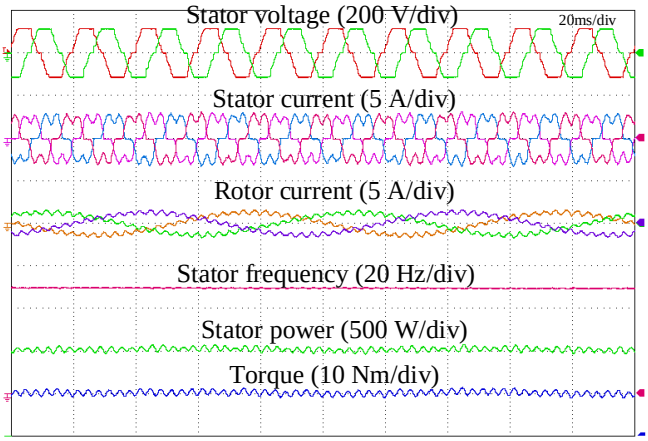

Fig. 14. Steady state results without improved direct resonant control.

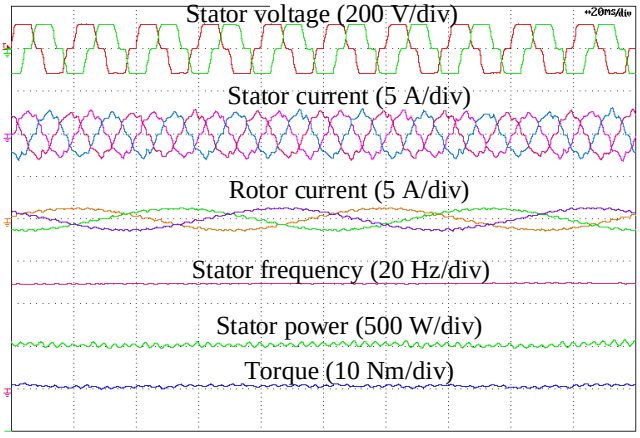

Fig. 15. Steady state results with improved direct resonant control.

The steady state results with improved direct resonant control is shown in Fig. 15. The 5th and 7th harmonic current are both greatly reduced to 2.3% and 5.8%. The harmonic current can not be totally suppressed due to the harmonic current necessary for reducing torque ripple. The 300 Hz torque ripple is also reduced to 0.93%. Thus, the improved direct resonant control can still be directly applied in the novel stator frequency and power control, which is simple and effective in mitigating both the torque ripple and harmonic currents. After mitigating the stator harmonic currents, the operation loss of DFIG is reduced and the efficiency of DFIG-DC system is improved.

VI. Conclusion

A novel stator power and stator frequency control method of DFIG-DC system based on air gap flux orientation is proposed in this paper. Instead of adopting voltage model or current model for acquiring the stator frequency and orientation angle, the stator power control loop is applied for generating the stator frequency and orientation angle, which can avoid the parameter dependency and dc sampling offset effect. The air gap flux orientation method is achieved through controlling *q*-axis exciting current to be zero. Furthermore, the improved direct resonant control for mitigating torque ripple and harmonic currents can still be directly used which indicates the newly proposed control strategy is suitable for all the existing improved control strategy for suppressing harmonics or improving efficiency. This control strategy reduces parameter dependencies without loss of existing control performance.

References

[1] G. D. Marques and M. F. Iacchetti, "DFIG Topologies for DC Networks: A Review on Control and Design Features," *IEEE Trans. Power Electron*, vol. 34, no. 2, pp. 1299-1316, Feb. 2019.

[2] T. Dragicevic, X. Lu, J. C. Vasquez, and J. M. Guerrero, "DC microgrids— Part I: A review of control strategies and stabilization techniques," *IEEE Trans. Power Electron.*, vol. 31, no. 7, pp. 4876–4891, Jul. 2016.

[3] N. Yu, H. Nian, and Y. Quan, "A novel DC grid connected DFIG system with active filter based on predictive current control," *in Proc. Int. Conf. Elect. Mach. Syst.*, Aug. 22–23, 2011, pp. 4525–4537.

[4] H. Nian and X. Yi, "Coordinated control strategy for doubly-fed induction generator with dc connection topology," *IET Renew. Power Gener.*, vol. 9, no. 7, pp. 747–756, Aug. 2015.

[5] M. F. Iacchetti, G. D. Marques, R. Perini, "Operation and design issues of a DFIG stator-connected to a DC-Net by a diode rectifier," *IET Electr. Power Appl.*, vol 8, no. 8, pp. 310-319, Sep. 2014.

[6] G. D. Marques and M. F. Iacchetti, "Stator frequency regulation in a field oriented controlled DFIG connected to a DC Link," *IEEE Trans. Ind Electron.*, vol. 61, no. 11, pp. 5930-5939,Nov. 2014.

[7] G. D. Marques, M. F. Iacchetti, "Inner control method and frequency regulation of a DFIG connected to a DC link," *IEEE Trans. Energy Convers.*, vol.29, no.2, pp.435-444, Jun. 2014.

[8] M. F. Iacchetti, G. D. Marques, and Roberto Perini, "Torque ripple reduction in a DFIG-DC system by resonant current controllers," *IEEE Trans. Power Electron.*, Vol.30, No.8, pp. 4244-4254, Aug. 2015.

[9] H. Nian, C. Wu, and P. Cheng, "Direct resonant control strategy for torque ripple mitigation of DFIG connected to DC link through diode rectifier on stator," *IEEE Trans. Power Electron.*, vol. 32, no. 9, pp. 6936–6945, Sep. 2017.

[10] G. D. Marques and M. F. Iacchetti, "A self-sensing stator-current-based control system of a DFIG connected to a DC-Link", *IEEE Trans. Ind Electron.*, Vol. 62, No. 10, pp. 6140-6150, Oct. 2015.

[11] C. Wu and H. Nian, "Sinusoidal current operation of DFIG-DC System without stator voltage sensors," *IEEE Trans. Ind. Electron.*, vol. 65, no. 8, pp. 6250–6258, Aug. 2018.

[12] C. Wu, H. Nian, "An improved repetitive control of DFIG-DC system for torque ripple suppression," *IEEE Trans. on Power Electron.*, vol. 33, no.9, pp. 7634-7644, Sep. 2018.
[13] H. Misra, A. Gundavarapu, and A. K. Jain, "Control scheme for DC voltage regulation of stand-alone DFIG-DC system," *IEEE Trans. Ind. Electron.*, vol. 64, no. 4, pp. 2700–2708, Apr. 2017.
[14] H. Misra and A. K. Jain, "Analysis of stand alone DFIG-DC system and DC voltage regulation with reduced sensors," *IEEE Trans Ind. Electron.*, vol. 64, no. 6, pp. 4402–4412, Jun. 2017.
[15] H. Misra and A. K. Jain, "Mathematical modelling and control of standalone DFIG-DC system in rotor flux reference frame," *IEEE Trans. Ind.Electron.*, vol. 65, no. 5, pp. 3708–3717, May 2018.
[16] G. D. Marques and M. F. Iacchetti, "Minimization of torque ripple in the DFIG-DC system via predictive delay compensation," *IEEE Trans. Ind. Electron.*, vol. 65, no. 1, pp. 103–113, Jan. 2018.
[17] S. M. A. Cruz, G. D. Marques, P. F. C. Gonc¸alves, and M. F. Iacchetti, "Predictive torque and rotor flux control of a DFIG-dc system for torqueripple compensation and loss minimization," *IEEE Trans. Ind. Electron.*, vol. 65, no. 12, pp. 9301-9310, Dec. 2018.
[18] C. Wu and H. Nian, "Improved direct resonant control for suppressing torque ripple and reducing harmonic current losses of DFIG-DC system," *IEEE Trans. Power Electron*, vol. 34, no. 9, pp. 8739-8748, Sep. 2019.

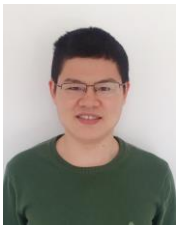

Chao Wu (M'19) was born in Hubei Province, China. He received the B.Eng. degree from HeFei University of Technology, Hefei, China and the Ph.D. degree from Zhejiang University, Hangzhou, China, in 2014 and 2019, both in electrical engineering. He is currently a Postdoctoral Researcher in the Department of Energy Technology, Aalborg University, Aalborg, Denmark.
His current research interests include cooperative control of multi-converter systems, particularly the control and operation of doubly fed induction generators for DC connection.

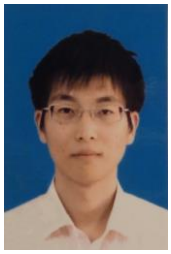

Dao Zhou (S'12-M'15-SM'19) received the B.S. from Beijing Jiaotong University, Beijing, China, in 2007, the M. S. from Zhejiang University, Hangzhou, China, in 2010, and the Ph.D. from Aalborg University, Aalborg, Denmark, in 2014, all in electrical engineering.
Since 2014, he has been with Department of Energy Technology, Aalborg University, where currently he is an Assistant Professor. His research interests include modeling, control, and reliability of power electronics in renewable energy application.
Dr. Zhou received the Renewable and Sustainable Energy Conversion Systems of the IEEE Industry Applications Society First Prize Paper Award in 2015, and Best Session Paper at Annual Conference of the IEEE Industrial Electronics Society (IECON) in Austria in 2013.

Peng Cheng was born in Liaoning Province, China. He received the B.S. and Ph.D. degree from Zhejiang University, Hangzhou, China, in 2011 and 2016, both in electrical engineering. He is currently an assistant professor in the Department of China Institute of Energy and Transport Integration Development, North China Electric Power University, China.
His current research interests include multi-converter power systems and renewable power generation, particularly wind power generation.

Frede Blaabjerg (S'86–M'88–SM'97–F'03) was with ABB-Scandia, Randers, Denmark, from 1987 to 1988. From 1988 to 1992, he got the PhD degree in Electrical Engineering at Aalborg University in 1995. He became an Assistant Professor in 1992, an Associate Professor in 1996, and a Full Professor of power electronics and drives in 1998. From 2017 he became a Villum Investigator. He is honoris causa at University Politehnica Timisoara (UPT), Romania and Tallinn Technical University (TTU) in Estonia.
His current research interests include power electronics and its applications such as in wind turbines, PV systems, reliability, harmonics and adjustable speed drives. He has published more than 600 journal papers in the fields of power electronics and its applications. He is the co-author of four monographs and editor of ten books in power electronics and its applications.
He has received 32 IEEE Prize Paper Awards, the IEEE PELS Distinguished Service Award in 2009, the EPE-PEMC Council Award in 2010, the IEEE William E. Newell Power Electronics Award 2014, the Villum Kann Rasmussen Research Award 2014, the Global Energy Prize in 2019 and the 2020 IEEE Edison Medal. He was the Editor-in-Chief of the IEEE TRANSACTIONS ON POWER ELECTRONICS from 2006 to 2012. He has been Distinguished Lecturer for the IEEE Power Electronics Society from 2005 to 2007 and for the IEEE Industry Applications Society from 2010 to 2011 as well as 2017 to 2018. In 2019-2020 he serves a President of IEEE Power Electronics Society. He is Vice-President of the Danish Academy of Technical Sciences too.
He is nominated in 2014-2019 by Thomson Reuters to be between the most 250 cited researchers in Engineering in the world.